

# Global-Local Interface with Selective Direct and Singularity-Avoiding Motion Mapping for Intuitive Teleoperation

Jianshu Zhou<sup>\*#</sup>, *Member, IEEE, ASME*, Boyuan Liang<sup>#</sup>, *Student Member, IEEE*, Junda Huang, Ian Zhang, Zhengyang Liu, Pieter Abbeel, *Fellow, IEEE*, Masayoshi Tomizuka<sup>\*</sup>, *Life Fellow, IEEE, ASME*

**Abstract**—This paper presents the Global-Local (G-L) Teleoperation Interface, a hierarchical framework that enhances human-robot interaction by decoupling large-scale manipulator positioning from fine end-effector manipulation. The global component enables efficient workspace traversal, while the local component facilitates precise and dexterous maneuvering. To address kinematic singularities on the slave side—particularly during local fine manipulation—we propose a singularity-avoiding motion mapping strategy that improves both stability and intuitiveness. Additionally, we introduce the concept of an operational Jacobian to formally analyze the smoothness of slave joint motions under local control. The G-L interface is realized in two variants: Direct Mapping and Singularity-Avoiding Mapping. Both implementations are validated through hardware experiments involving tasks that demand precision, extended linear motion, and large orientation changes. Results demonstrate significant improvements in task success rate, execution efficiency, and user experience compared to conventional systems relying solely on global or local control. These findings indicate that the G-L interface offers a robust and scalable foundation for intuitive and versatile teleoperation across complex tasks and unstructured environments.

**Index Terms**—Teleoperation, Human-Robot Interface, Kinematic Mapping, Singularity Avoidance

## I. INTRODUCTION

Teleoperation serves as a critical human-robot interface paradigm, enabling remote robotic operation in scenarios where human manual manipulation is insufficient or unsafe, such as surgery, disaster response, and exploration in hazardous or unstructured environments [1]–[8]. It also plays an increasingly essential role in data-driven robotic learning, where high-quality human demonstration datas are crucial for imitation learning and multimodal policy training [9]–[16].

Despite extensive research, existing teleoperation frameworks exhibit fundamental trade-offs among dexterity, workspace range, and intuitiveness. One common approach employs six-DoF tracking of the operator’s hand using floating controllers or vision-based systems [17]–[26]. These enable freehand dexterity but often lack physical correspondence with the slave robot’s workspace, leading to non-intuitive motion mapping and vulnerability against manipulator singularities.

Alternatively, kinematically matched master devices replicate the structure of the slave robot using a scaled joint-link chain, or in some cases, by employing an identical slave device as the master itself [27]–[31]. This improves mapping of reachable configurations and collision awareness. However, such systems often constrain the operator’s movements and suffer from encoder detent torque, mechanical friction, and limited fidelity during fine manipulation.

To overcome these limitations, we propose the Global-Local (G-L) Teleoperation Interface (Fig. 1), a framework that hierarchically decouples human input into two synergistic control pathways: a global controller for large-scale positioning and a local controller for high-precision end-effector manipulation. This modular design fuses joint space awareness and dexterous control while minimizing the drawbacks of traditional systems. The G-L interface is a general teleoperation framework that supports flexible combinations of global and local master devices, allowing system configurations to be tailored to diverse tasks and hardware platforms. In addition, to facilitate more intuitive orientation control and avoid the impact of manipulator singularity while the local component is activated, we introduce a practical singularity-avoiding motion mapping strategy targeting the Pieper kinematics structure [32] between the local component motion and slave system’s joints. A concept termed *operational Jacobian* is proposed to give a rigorous mathematical argument of why this singularity-avoiding motion mapping ensures smooth slave joint motions at manipulator singularities. This concept can also be generalized to analyze the teleoperation control on slave systems other than Pieper structures.

Experimental validation and demonstration of the G-L interface utilized two different implementations defined by the mapping from the local component to the slave system’s joints. The first, designated *Direct Mapping*, maps the scaled Cartesian motion of the local component directly to the slave end-effector. This preserves six degrees of freedom for local manipulation but is characterized by less intuitive orientation mapping and the absence of a singularity avoidance feature. In contrast, the second implementation, *Singularity-Avoiding Mapping*, employs the aforementioned manipulator singularity avoidance technique. Although this method reduces the available degrees of freedom by one, it provides more intuitive orientation mapping and robustly avoids singularities within its designated workspace.

The contributions of this work are summarized as follows.

<sup>\*</sup>Corresponding to Jianshu Zhou and Masayoshi Tomizuka. (jianshuzhou@berkeley.edu; tomizuka@berkeley.edu)

<sup>#</sup>These authors contributed equally to this work.

<sup>1</sup>Department of Mechanical Engineering, University of California, Berkeley, CA 94720, USA

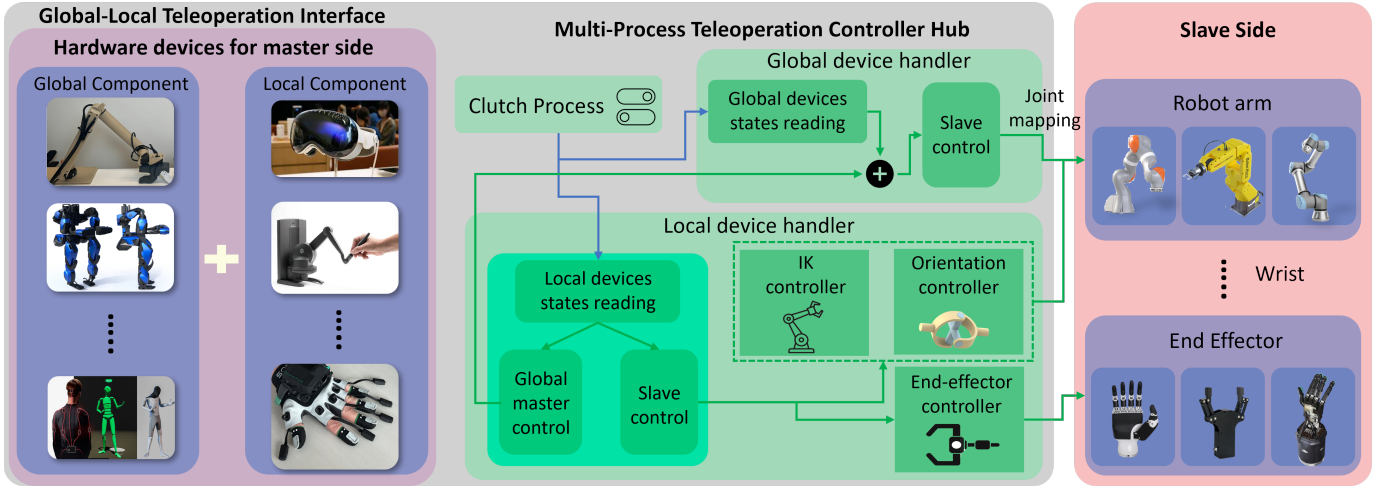


Fig. 1. Comparison of teleoperation interfaces across different system configurations. Our proposed G-L interface (both bimanual and single-arm variants) offers broader joint-space coverage and higher precision, while retaining compatibility with complex end-effectors.

- 1) **Proposal of the G-L Teleoperation Interface:** A hierarchical architecture that decouples large-scale positioning from fine end-effector manipulation, designed to enhance operational flexibility and task-specific performance.
- 2) **Implementation of Two Interface Realizations:** Development and demonstration of the G-L concept through two distinct hardware implementations: the *Direct Mapping Realization* and the *Singularity-Avoiding Realization*. The latter introduces a specialized motion mapping strategy for the local control component, aimed at improving orientation control intuitiveness and ensuring stable operation near slave manipulator singularities.
- 3) **Introduction of the Operational Jacobian:** Proposal of the *operational Jacobian* as a mathematical tool to rigorously analyze the smoothness of the slave system's joint motion during teleoperation.
- 4) **Experimental Validation and Comparative Analysis:** Comprehensive validation of the G-L interface through experiments involving precision manipulation, large linear movements, and significant angular adjustments. Results demonstrate quantifiable improvements in success rates, operational efficiency, and user experience compared to conventional single-mode (global-only or local-only) systems.

The remainder of this paper is organized as follows. Section II introduces the proposed Global-Local (G-L) teleoperation interface and its key design criteria. Section III details the direct mapping realization, while Section IV presents the singularity-avoiding mapping strategy. Section V describes the operational Jacobian tool. Experimental validations across various manipulation tasks are discussed in Section VI. Finally, Section VII concludes the paper with a summary of contributions, limitations, and directions for future work.

## II. GLOBAL-LOCAL TELEOPERATION INTERFACE

To be considered a valid implementation of the G-L Interface, a decoupled master system must adhere to the following

criteria. First, the global component must provide an intuitive and comprehensive representation of the slave system's collision configuration. It should enable rapid, large-amplitude adjustments of the slave's pose, prioritizing efficient workspace navigation over fine manipulation or dexterity. Second, the local component must facilitate precise, fine-grained control of the slave's end-effector, enabling the operator to execute tasks requiring dexterity and accuracy. It should prioritize the seamless transfer of the operator's manipulation skills to the slave system, with less emphasis on reflecting the slave's overall configuration or controlling all DoFs. In the remaining of this paper, without further clarification, our discussions are limited to slave systems with serial connected structure.

Employing a scaled replica of the slave system, a common strategy in teleoperation [9], [30], effectively meets the requirements for the global component of our system. However, this implementation differs from existing scaled replica teleoperation systems in two ways. Firstly, the global component does not require exact kinematic correspondence with the slave system's revolute axes, as its primary function is to enable rapid and coarse motions. It only needs to provide an approximation of the current slave system's collision configuration, allowing the human operator to avoid potential collisions during coarse adjustments of the slave's pose. Secondly, the global component need not encompass all Degrees of Freedom (DoFs) of the slave system. It is generally observed that DoFs closer to the base exert a more substantial influence on both the robot's end-effector position and its overall collision state compared to DoFs nearer the end-effector. Consequently, it may be sufficient for the global component to replicate only these more influential, base-proximal DoFs.

Tracking the operator's hand motion represents a suitable approach for implementing the local component of the interface. A key challenge in Global-Local (G-L) interface design is establishing an intuitive motion mapping between this local component and the slave system. Focusing on the widely applied Pieper kinematics manipulator structure, we propose two distinct motion mapping methods. The first, more direct



method involves mapping the local component's motion to the slave system's end-effector motion and solving for the required joint poses using inverse kinematics. Owing to its straight-forward implementation and preservation of all 6 DoFs for the slave end-effector, this technique is commonly adopted in robot data collection applications [25]. However, if the initial orientation of the local component does not align well with the slave end-effector's starting orientation, this method can prove counter-intuitive for orientation control. Furthermore, manipulator singularities can adversely affect the usability of the local component, an issue detailed further in Section IV. The second method maps the three rotational DoFs of the local component to three mutually perpendicular slave joints and locks one slave DoF to mitigate certain rotational singularities. While this approach reduces the effective mapped DoFs by one, it provides considerably more intuitive orientation control.

Using the two local motion mapping approaches and with different number of DoFs the global components cover, we present the Direct Mapping and Singularity-Avoiding Mapping realizations of the G-L interface, which will be introduced in detail in sections III and IV. Both realizations share a challenge during the transition from the local to global component. A mismatch can arise between the pose of the scaled replica (global component) and the actual slave system configuration, potentially causing an abrupt motion in the slave upon returning to global control. To mitigate this, the global component assumes a "slave" role during local component activation, mirroring the joint motions of the true slave system. This ensures pose synchronization between the global component and the slave, facilitating a smooth transition when switching back to global controls.

Fig. 2 illustrates a representative configuration of the proposed Global-Local (G-L) interface. Haptic devices are used to capture the operator's fine hand motions, while a scaled-down 3-DOF joint-link chain captures the large range arm movement. Two pairs of foot pedals allow the operator to switch between global and local control modes.

### III. DIRECT MAPPING OF LOCAL COMPONENT MOTION

It is important to emphasize the key distinction between the Direct Mapping and Singularity-Avoiding Mapping strategies: they primarily differ in the local motion mapping method and the number of degrees of freedom allocated to the global component.

The global component of the Direct Mapping implementation covers the full six DoFs in the Pieper structure slave robot [33]–[35]. Activating the global component places the slave system in joint control mode, replicating the scaled replica's joint positions within the limits of the motor capacities. Conversely, activating the local component switches the slave system to end-effector Cartesian control, where it tracks the motion of the haptic device.

To facilitate precise control of the end-effector, the slave system is designed to track only a portion of the local component motion. Denote the slave end-effector pose with  $(\mathbf{p}, \mathbf{R})$  where  $\mathbf{p} \in \mathbb{R}^3$  is the position and  $\mathbf{R} \in \mathbb{R}^{3 \times 3}$  is the orientation represented by a rotational matrix. Let  $\mathbf{q}$  be the joint poses of

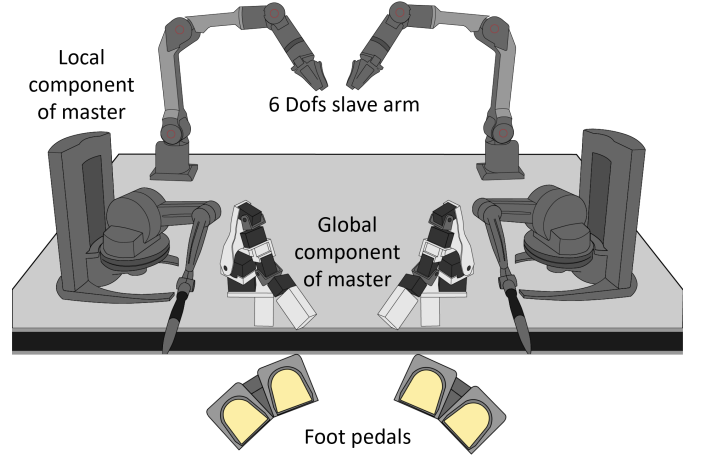


Fig. 2. A schematic diagram of G-L interface. The global component is a scaled replica of the slave robot and the local component is a haptic device. The two step pedals allows the operator to rapidly switch between the local and global component. If the local component is activated, the global component will temporarily turn into a slave system that follows the actual slave system to avoid joint position mismatch when switching back to the global component.

the slave robot, then we have  $\mathbf{q} = \mathbf{F}(\mathbf{p}, \mathbf{R})$  where  $\mathbf{F}$  is the inverse kinematics of Pieper kinematics structure, which can be efficiently computed in closed form [32].

Every time the local component is activated, its starting pose  $(\mathbf{p}_0^m, \mathbf{R}_0^m)$  as well as the slave end-effector's starting pose  $(\mathbf{p}_0^s, \mathbf{R}_0^s)$  will be recorded. Suppose at a certain moment  $t$ , the local component moves to pose  $(\mathbf{p}_t^m, \mathbf{R}_t^m)$ , we first compute the linear and rotational displacements since activation.

$$\begin{aligned} d\mathbf{p}_t^m &= \mathbf{p}_t^m - \mathbf{p}_0^m \\ (\mathbf{l}_t^m, \theta_t^m) &= \mathbf{G}(d\mathbf{R}_t^m) = \mathbf{G}(\mathbf{R}_0^{m,T} \mathbf{R}_t^m) \end{aligned} \quad (1)$$

where the superscript  $T$  stands for transpose and  $\mathbf{G}$  maps the rotational matrix to axis-angle format.  $\mathbf{l}_t$  is the normalized rotational axis direction and  $\theta_t$  is the angle.

Given prespecified linear and rotational scaling factors  $\alpha_l, \alpha_r \in (0, 1]$ , the slave system will move its end-effector pose towards the scaled linear and rotational displacements of the haptic device. Mathematically, the target slave pose at moment  $t$  is

$$\begin{aligned} \mathbf{p}_t^s &= \mathbf{p}_0^s + \alpha_l d\mathbf{p}_t^m \\ \mathbf{R}_t^s &= \mathbf{R}_0^s \mathbf{G}^{-1}(\mathbf{l}_t^m, \alpha_r \theta_t^m) \end{aligned} \quad (2)$$

with  $\mathbf{G}^{-1}$  being the mapping that gets the rotational matrix from the axis-angle interpretation.

With the generated end-effector pose, the target joint poses of the slave robot at moment  $t$  will be

$$\mathbf{q}_t^s = \mathbf{F}(\mathbf{p}_t^s, \mathbf{R}_t^s) \quad (3)$$

### IV. SINGULARITY-AVOIDING MAPPING OF LOCAL COMPONENT MOTION

Despite the preservation of full degrees of freedom of the end-effector, the aforementioned direct motion mapping has two major limitations.

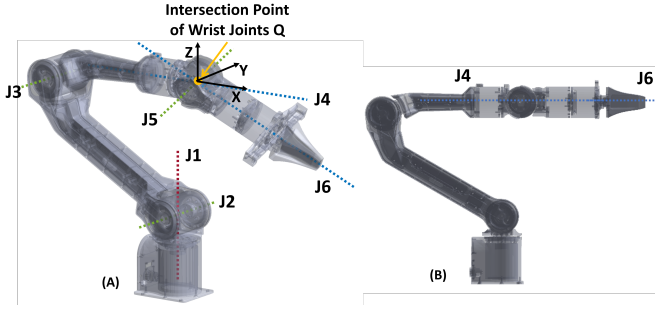


Fig. 3. (A) Pieper Kinematics Structure using Agile X Piper as an example. (B)  $q_5 = 0^\circ$  wrist singularity, which is a typical manipulation pose and is also the singularity type we are focusing on avoiding.

- It is particularly vulnerable against manipulator singularities, especially the wrist singularity in Pieper kinematics, which can happen everywhere inside the manipulator reachable workspace [36]. This demands human operators to pay extra attention on the slave joint poses other than the end-effector pose.
- When the starting orientation of the local component and the slave end-effector have an obvious misalignment, controlling orientation using direct mapping can be overwhelming for human operators. This is because it is difficult for human operators to predict the slave end-effector's orientation change given the motion of the local component. Additionally, they cannot intuitively discern which joints will be actuated and how much they will move.

This section focuses on the scenario when the slave system has a Pieper kinematic structure and proposes a practical local component motion mapping method to alleviate these limitations.

#### A. Pieper Kinematics and Translation-Rotation Decoupling

Pieper kinematics structure, also known as the 321 kinematics structure, is widely adopted in 6-joint industrial robot arms for its closed-form inverse kinematics. Fig. 3 is an illustration of the three most important characteristics of Pieper kinematics structure using AgileX Piper as an example.

- The base joint (J1) and the first shoulder joint (J2) intersect and are perpendicular.
- The two shoulder joints (J2 and J3) are parallel.
- The three wrist joints (J4, J5 and J6) intersect at the same point  $Q$ , usually arranged in an intrinsic X-Y-X Euler Angles order.

It can be observed that the intersection point  $Q$  is relatively close to the end-effector tip and its position is only affected by the poses of the base and shoulder joints. In addition, since the three wrist joints formulate an Euler angle combinations, they can dexterously adjust the end-effector orientation in a nonzero-measure set without actuating J1, J2 and J3, regardless of the Cartesian position of  $Q$  [37]. With this observation, the following amendments are made to the Direct Mapping realization.

- Translation of the local component now controls the linear motion of the intersection point  $Q$ ,  $p_t^Q$ , not the

end-effector's linear motion  $p_t^s$ . Therefore, only J1, J2 and J3 will be actuated.

- Rotation of the local component still controls the slave end-effector's orientation  $R_t^s$ , but only J4, J5 and J6 will be actuated.

Denote the starting pose of point  $Q$  as  $(p_0^Q, R_0^Q)$ , the target position of point  $Q$  at moment  $t$  will be

$$p_t^Q = p_0^Q + \alpha_l dp_t^m \quad (4)$$

The joint poses are now solved as

$$\begin{aligned} [q_{1,t}^s, q_{2,t}^s, q_{3,t}^s]^T &= F_{123}(p_t^Q) \\ [q_{4,t}^s, q_{5,t}^s, q_{6,t}^s]^T &= F_{456}(R_t^Q, R_t^s) \end{aligned} \quad (5)$$

where  $F_{123} : \mathbb{R}^3 \rightarrow \mathbb{R}^3$  is the mapping from the  $Q$  point position to J1, J2 and J3 joint poses.  $F_{456} : \mathbb{R}^{3 \times 3} \rightarrow \mathbb{R}^3$  maps from rotation matrix to J4, J5 and J6 joint poses.  $R_t^Q$  is the current orientation of point  $Q$ .

This decoupling process of the local component's translation and rotation partially reduces the corresponding number of joints of each local component DoF to less than or equal to three. Although this increases control intuitiveness for human operators, it still suffers from manipulator singularities. In section IV-B, we discuss further amendments that can help avoid manipulator singularities.

#### B. Singularities in Pieper Kinematics

Following notations in [36], the motion mapping from the configuration space to the operational space has the following form.

$$v_t^e = J(q_t) \dot{q}_t \quad (6)$$

An important difference here is that  $v_t^e$  now consists of the linear velocity of point  $Q$  and the angular velocity of the end-effector  $v_t^e = [\dot{p}_t^Q \ \omega_t^e]^T$ . Since Pieper kinematics structure has six independent joints, the Jacobian can be naturally partitioned into  $(3 \times 3)$  blocks.

$$J(q_t) = \begin{bmatrix} J_{11}(q_t) & J_{12}(q_t) \\ J_{21}(q_t) & J_{22}(q_t) \end{bmatrix} \quad (7)$$

Manipulator singularities are the joint configurations  $q$  where the matrix  $J(q)$  presents a zero singular value. When  $J(q)$  is a square matrix, this is equivalent to having a zero determinant,  $\det J(q) = 0$ . Since the position  $p_t^Q$  is independent of J4-J6, we know that  $J_{12}(q_t) = O_3$ . As a result, manipulator singularities can be identified from the following equation.

$$\det J_{11}(q) \det J_{22}(q) = 0 \quad (8)$$

Scenarios when  $\det J_{11}(q) = 0$  is often referred to as arm singularities since it mainly affects the linear velocity and  $\det J_{22}(q) = 0$  is often referred to as wrist singularities since it mainly affect angular velocities.  $J_{11}(q)$  and  $J_{22}(q)$  can be written in the form.

$$\begin{aligned} J_{11}(q) &= \begin{bmatrix} ((p^Q - p_1^J) \times \xi_1(q))^T \\ ((p^Q - p_2^J) \times \xi_2(q))^T \\ ((p^Q - p_3^J) \times \xi_3(q))^T \end{bmatrix}^T \\ J_{22}(q) &= [\xi_4(q) \ \xi_5(q) \ \xi_6(q)] \end{aligned} \quad (9)$$

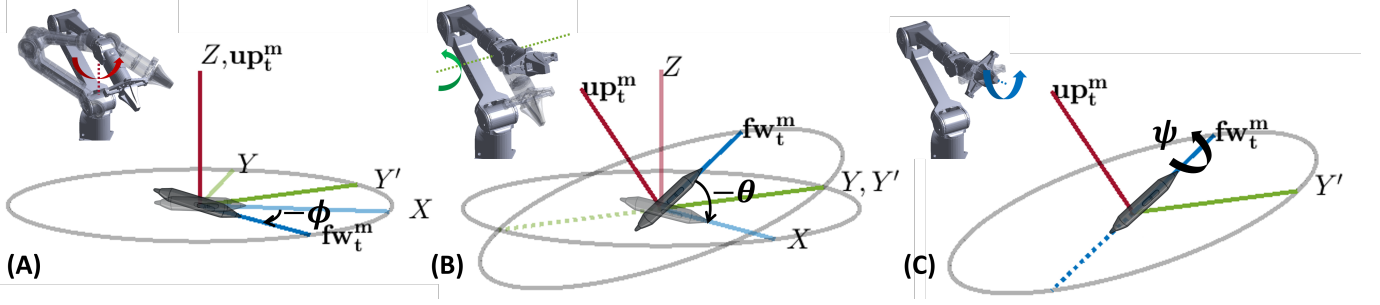


Fig. 4. Visualization of Singularity Avoidance Motion Mapping. The digital pen in the center indicates the direction where the local component is pointing to. (A) Row angle  $d\theta_t^m$  maps to J1 motion. Notice that under motion mapping (11), the digital pen does not necessarily align with the X-axis at the beginning. (B) Pitch angle  $d\phi_t^m$  maps to J5 motion. (C) Yaw angle  $d\psi_t^m$  maps to J6 motion.

where  $\xi_i(q)$ ,  $i = 1 \dots, 6$  is the unit vector pointing to the rotational direction of axis  $J_i$  and  $p_i^j$ ,  $i = 1 \dots 6$  are any random points on axis  $J_i$ . Since J4 is perpendicular to J5 and J5 is perpendicular to J6,  $J_{22}(q) = 0$  only when J4 is parallel to J6, which happens whenever  $q_5 = 0$ , as shown in Fig. 3B. One important arm singularity is when  $p^Q - p_2^j$  and  $p^Q - p_2^j$  are parallel, happening when  $q_3 = 0, \pm 180^\circ$ . These are usually called elbow singularities [36].

Arm singularities forms a well-identified set of points in the reachable space  $\mathcal{RS}^Q$  of point  $Q$ , so they can be suitably and intuitively avoided by the human operator. Wrist singularities, on the other hand, can be encountered everywhere in the reachable space  $\mathcal{RS}^Q$ , making it overwhelming for the human operator to intentionally avoid them [36]. Thus, in this work, we focus on finding a motion mapping to avoid wrist singularities. In section IV-C, we will discuss this singularity-avoiding motion mapping in detail.

### C. Singularity-Avoiding Motion Mapping

We first lock J4 at  $q_4 = 0$  and generate the Z-Y-X Euler angle leading to  $dR_t^m$ . Let  $H$  be the mapping from the a given rotation matrix to the Z-Y-X Euler angles.

$$\begin{bmatrix} \theta_t^m & \phi_t^m & \psi_t^m \end{bmatrix} = H(R_t^m) \quad (10)$$

$$\begin{bmatrix} \theta_0^m & \phi_0^m & \psi_0^m \end{bmatrix} = H(R_0^m)$$

Then, instead of asking the end-effector to follow the rotational translation  $dR_t^m$ , we directly add the scaled Euler angles to the target J1, J5, and J6 poses.

$$\begin{aligned} q_{1,t} &= q_{1,t-1} + \alpha_r(\theta_t^m - \theta_0^m) \\ q'_{5,t} &= q'_{5,t-1} + \alpha_r(\phi_t^m - \phi_0^m) \\ q_{6,t} &= q_{6,t-1} + \alpha_r(\psi_t^m - \psi_0^m) \end{aligned} \quad (11)$$

$q_{1,t}$  and  $q_{5,t}$  have been resolved in (11) and  $q_{5,t} = q'_{5,t} + q_{2,t} + q_{3,t}$ . Notice that this is different from computing  $[d\theta_t^m \ d\phi_t^m \ d\psi_t^m] = H(dR_t^m)$  and adding them to  $q_{1,t}$ ,  $q'_{5,t}$  and  $q_{6,t}$ .

Without loss of generality, let the local x-direction and y-direction respectively be the normalized *master forward vector* and *master upward vector*.

$$\begin{aligned} fw_t^m &= \cos \phi_t^m e_x + \sin \phi_t^m e_y \\ up_t^m &= e_z \end{aligned} \quad (12)$$

where  $e_x$ ,  $e_y$  and  $e_z$  are respectively X, Y, and Z direction unit vectors in world frame. Similarly, we also define the normalized *slave forward vector* and *slave upward vector*.

$$\begin{aligned} FW_t^s &= \cos \phi_t^s e_x + \sin \phi_t^s e_y \\ UP_t^s &= e_z \end{aligned} \quad (13)$$

$q_{2,t}$  and  $q_{3,t}$  should satisfy

$$\begin{aligned} (p_t^Q - p_0^Q) \cdot FW_t^s &= \alpha_l dp_t^m \cdot fw_t^m \\ (p_t^Q - p_0^Q) \cdot UP_t^s &= \alpha_l dp_t^m \cdot up_t^m \end{aligned} \quad (14)$$

where  $p_t^Q$  depends on  $q_{1,t}$ ,  $q_{2,t}$  and  $q_{3,t}$  while  $q_{1,t}$  is known. (14) can be easily solved using trigonometry, and this process is singularity-free for most robot configurations. Finally,  $q_{5,t}$  is obtained by

$$q_{5,t} = q'_{5,t} - q_2 - q_3 \quad (15)$$

Since (11) depends on the local component's relative motion, although mapping  $H$  has singularity when  $\theta_0^m$  or  $\theta_t^m = \pm 90^\circ$ , the user can easily avoid this point via resetting the starting master pose  $R_0^s$ . The simple additions in (11) and (15) indicates that as long as  $\theta_t^m$  or  $\theta_0^m$  in the local component are kept away from  $\pm 90^\circ$ , the slave system motion will always be smooth even in wrist singularities.

An important property of the motion mapping in (10) and (11) is that if the starting pose of the local component  $R_0^m$  aligns with the slave end-effector  $R_0^s$ , then they will be pointing at the same direction at all time,  $fw_t^m = FW_t^s$ , if  $\alpha_r = 1$ .

However, this singularity avoidance mapping comes with a price, that being the lose of the J4 DoF.  $q_4$  will be maintained at zero throughout local control. Unfortunately, as argued in section IV-B, if J4 is released and  $q_5$  is very close to zero, a random orientation-preserved linear motion with small amplitude of the local component will cause a large movement of the slave system. Therefore, the authors believe that developing a local motion mapping that preserves all 6 DoFs of the slave end-effector while maintaining smooth transitions at singularities requires new designs on the slave side. This will be discussed in detail in section VII.

### V. OPERATIONAL JACOBIAN IN TELEOPERATION

In this part, we give a more general and mathematically rigorous analysis of why the singularity-avoiding mapping can avoid wrist singularities.

Denote the generalized position of the master device with vectors  $\mathbf{P}$ , which can either be joint poses in the global component or the spatial position defined in the  $SE(3)$  set.  $\mathbf{q}$  is the generalized position of the slave system, which usually consists of the slave joint poses. We spot that relation between the master device motion  $\dot{\mathbf{P}} \in \mathbb{R}^n$  and slave side motion  $\dot{\mathbf{q}} \in \mathbb{R}^m$  often has the following form

$$\mathcal{F}(\mathbf{P})\dot{\mathbf{P}} = \mathbf{J}_o(\mathbf{P}, \mathbf{q})\dot{\mathbf{q}} \quad (16)$$

where  $\mathcal{F}(\mathbf{P}) \in \mathbb{R}^{\min(m,n) \times n}$  decreases dimension to handle the case when  $n > m$ . We name  $\mathbf{J}_o(\mathbf{P}, \mathbf{q}) : \mathbb{R}^n \times \mathbb{R}^m \rightarrow \mathbb{R}^{m \times m}$  the operational Jacobian, which can be used to indicate the smoothness of the motion mapping. The configuration that causes  $\mathbf{J}_o$  to have a zero singular value is called *operational singularity*, meaning that certain local component motion will cause indefinite joint motion in the slave system. For our local component, which is a haptic device, there is  $\dot{\mathbf{P}} = [\mathbf{v}^o \ \boldsymbol{\omega}^o]$ , where  $\mathbf{v}^o$  and  $\boldsymbol{\omega}^o$  are the stylus linear and angular velocities.

In direct motion mapping as shown in Section III, there are relations  $\mathbf{v}_i^o = \alpha_l \mathbf{v}_i$  and  $\boldsymbol{\omega}_i^o = \alpha_r \boldsymbol{\omega}_i$  from (2), indicating  $\mathcal{F}^{DM}(\mathbf{P}) = \mathbf{I}_6$  and the following relation between the operational Jacobian and manipulator Jacobian.

$$\mathbf{J}_o^{DM}(\mathbf{P}, \mathbf{q}_t) = \begin{bmatrix} \alpha_l \mathbf{I}_3 & \mathbf{O} \\ \mathbf{O} & \alpha_r \mathbf{I}_3 \end{bmatrix} \mathbf{J}_e(\mathbf{q}_t) \quad (17)$$

Therefore,  $\mathbf{J}_o^{DM}$  inherits all singularities of the manipulator Jacobian. Since  $\mathbf{J}_o^{DM}$  depends only on  $\mathbf{q}_t$ , it is infeasible to achieve smooth transition around singularities via adjusting the starting pose  $\mathbf{p}_0^m$ .

On the other hand, for the singularity avoidance mapping in section IV-C, since  $q_4$  is fixed at 0, we have  $m = 5$  and  $n = 6$ . Its operational Jacobian and projector can be written as the following

$$\mathbf{J}_o^{SA}(\mathbf{P}, \mathbf{q}) = \begin{bmatrix} 0 & A_{11} & A_{12} & 0 & 0 \\ 0 & A_{21} & A_{22} & 0 & 0 \\ 1 & 0 & 0 & 0 & \cos \theta_t^m \\ 0 & 0 & 0 & \sin \phi_t^m & \sin \theta_t^m \cos \phi_t^m \\ 0 & 0 & 0 & -\cos \phi_t^m & \sin \theta_t^m \sin \phi_t^m \end{bmatrix} \mathbf{W}$$

$$\mathcal{F}^{SA}(\mathbf{P}) = \begin{bmatrix} \cos \phi_t^m & \sin \phi_t^m & 0 & 0 & 0 & 0 \\ 0 & 0 & 1 & 0 & 0 & 0 \\ 0 & 0 & 0 & 1 & 0 & 0 \\ 0 & 0 & 0 & 0 & 1 & 0 \\ 0 & 0 & 0 & 0 & 0 & 1 \end{bmatrix}$$

$\mathbf{W}$  is a constant matrix generated from  $q_5' = q_5 + q_2 + q_3$ .

$$\mathbf{W} = \begin{bmatrix} 1 & 0 & 0 & 0 & 0 \\ 0 & 1 & 0 & 0 & 0 \\ 0 & 0 & 1 & 0 & 0 \\ 0 & 1 & 1 & 1 & 0 \\ 0 & 0 & 0 & 0 & 1 \end{bmatrix} \quad (18)$$

Letting the distance from J2 to J3 and the distance from J3 to Q to be  $l_2$  and  $l_3$  respectively, we have

$$\begin{aligned} A_{11} &= l_2 \sin q_2 - l_3 \sin(q_2 + q_3) \\ A_{12} &= -l_3 \sin(q_2 + q_3) \\ A_{21} &= l_2 \cos q_2 - l_3 \cos(q_2 + q_3) \\ A_{22} &= -l_3 \cos(q_2 + q_3) \end{aligned} \quad (19)$$

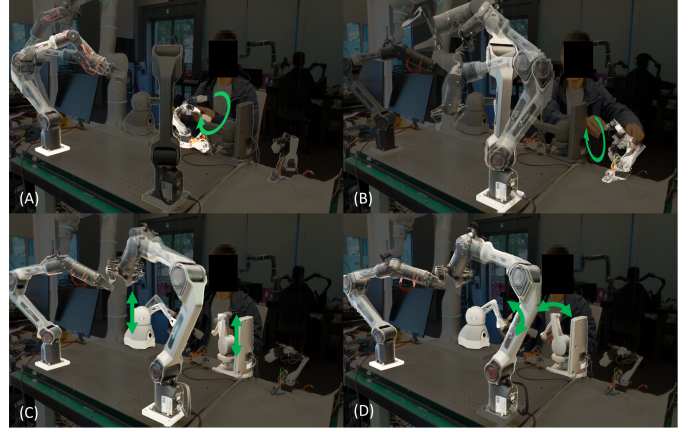


Fig. 5. Hardware setup of the Global-Local (G-L) teleoperation interface. (A), (B): Global teleoperation subsystem using a 3-DOF joint-link chain as the master device. (C), (D): Local teleoperation subsystem using a commercial haptic device as the master component.

Since  $\mathbf{W}$  and  $\mathcal{F}^{SA}(\mathbf{P})$  always have nonzero singular values, identifying the singularities in (V) is equivalent to identifying singularities of the following two submatrices.

$$\mathbf{A} = \begin{bmatrix} A_{11} & A_{12} \\ A_{21} & A_{22} \end{bmatrix} \quad \mathbf{B} = \begin{bmatrix} 1 & 0 & \cos \theta_t^m \\ 0 & \sin \phi_t^m & \cos \theta_t^m \cos \phi_t^m \\ 0 & -\cos \phi_t^m & \cos \theta_t^m \sin \phi_t^m \end{bmatrix}$$

$\mathbf{A}$  has zero singular value at the elbow singularity, which can be easily and intuitively avoided by the human operators.  $\mathbf{B}$  is singular when  $\theta_t^m = \pm 90^\circ$ . Interestingly,  $\theta_t^m$  here is the pitch angle of the local component instead of the slave end-effector. This means one can always reset the local component starting orientation  $\mathbf{R}_0^m$  to avoid  $\theta_t^m$  from reaching  $\pm 90^\circ$ . Therefore, singularities in  $\mathbf{B}$  is independent of slave joint poses  $\mathbf{q}$ , showing that wrist singularities is no longer impeding the teleoperation performance.

Motion mapping (16) covers a much wider range of teleoperation systems and does not require the master and slave systems to have the same DoF. Therefore, the idea of using operational Jacobians in analyzing the teleoperation system's robustness against manipulator singularities can also be generalized to teleoperation systems with different kinematic structures.

## VI. EXPERIMENTAL VALIDATIONS

This section presents experimental results validating the performance of G-L interface leveraging the direct motion mapping (Section III) and singularity-avoiding motion mapping (Section IV). The evaluation focuses on three key aspects:

- 1) **Precision Control:** Using direct motion mapping, we assessed the system's capability for high-accuracy telemanipulation through tasks with stringent precision requirements.
- 2) **Workspace Coverage:** Also employing direct motion mapping, we evaluated the ability to command extensive movements across the slave robot's workspace, demonstrating effective utilization of its kinematic limits.



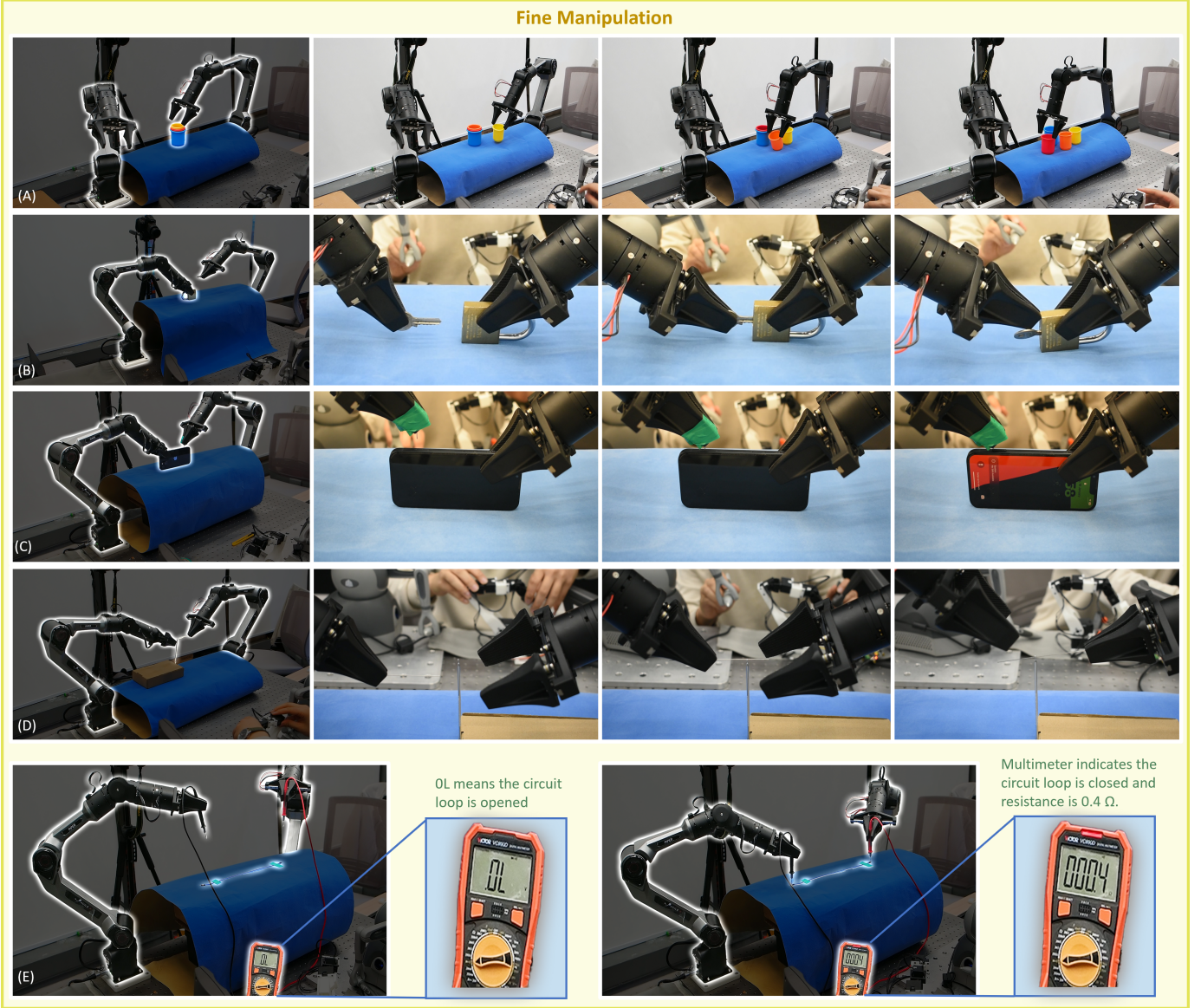


Fig. 6. Snapshots of tasks requiring precise manipulation. (A) Taking out Nested Buckets. (B) Key Insertion. (C) SIM Card Needle Insertion. (D) Needle Threading. (E) Wire Testing with Multimeter. The supplementary video of this paper shows the whole process of these demonstrations. Examples (B), (C), (D), and (E) feature bimanual fine manipulation, where both slave arms need to maintain precise position or orientation for completion.

### 3) Orientation Dexterity and Singularity Handling:

Utilizing the singularity-avoiding mapping, we demonstrated intuitive control during tasks involving significant orientation changes, specifically highlighting smooth trajectory execution during the traversal of wrist singularities.

In addition to these demonstrations, a quantitative comparison was conducted to assess the benefits of the proposed integrated Global-Local (G-L) interface. Task completion times for both fine-grained manipulation and large-range motion scenarios were measured using the full G-L interface and compared against performance when using only the global or local component in isolation. This analysis serves to quantify the advantages derived from combining these complementary components.

#### A. Implementation Details

The global components are actuated with Dynamixel XL330-M288 servomotors arranged to a desired joint-link chain mimicking the Pieper robot arms. For direct mapping, the global component has full 6 DoFs, and for local mapping, it has only 3 DoFs. Fig. 5 shows snapshots of G-L interface realization. The motion correspondence of the direct mapping and singularity-avoiding realizations can be found in the supplementary video. The local component comprises two 3D System 6-DoF Touch devices for precise end-effector control in Cartesian space. The isolated global components in the comparison experiments has 6 DoFs.

#### B. Precise Manipulation Demo

To assess the precision and dexterity afforded by the direct mapping teleoperation realization, we conducted a series



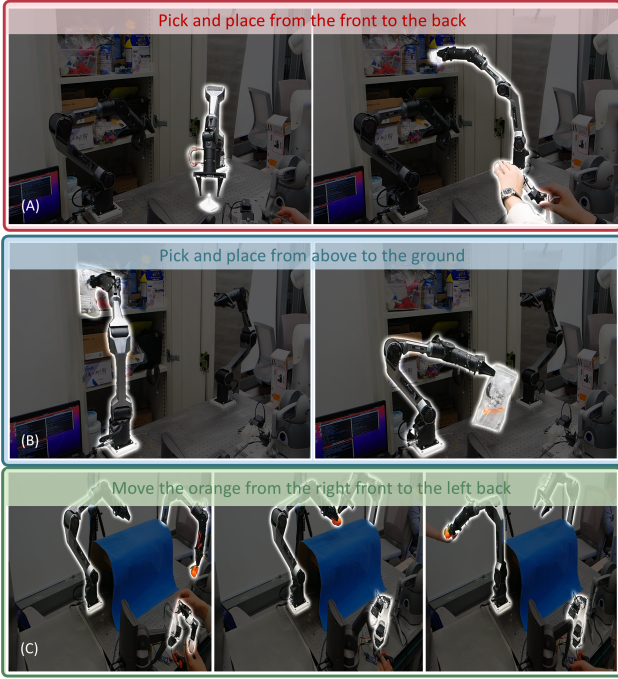


Fig. 7. Snapshots of tasks requiring large workspace. (A) Move an object from the desk to the cabinet. (B) Take a bag from the cabinet and place it on the desk. (C) Bimanual handling of oranges from the front-left of the workspace to the back-right. (D) Bimanual transferring a test tube from a wash basin to a rack. (E) Pouring the liquid from a test tube into a beaker, and then place the test tube back on the rack.

of experiments involving intricate manipulation tasks. These tasks, detailed below, were selected to represent challenges commonly encountered in real-world scenarios and to highlight the system’s capabilities in addressing them. Snapshots of these tasks are shown in Fig. 6.

- **Key Insertion:** This task, known for its demanding precision requirements, involves inserting a key into a standard bronze lock. The small tolerances between the key and lock necessitate precise control of both linear and rotational motion, as even minor deviations can result in failure or damage to the lock.
- **Needle Threading:** This bimanual task requires one slave arm to manipulate a fishing line through a needle eye with a radius of approximately 1.5 mm. The second slave arm then grasps the line and pulls it through, demonstrating coordinated manipulation and fine teleoperation.
- **Taking out Nested Buckets:** This task evaluates the system’s ability to manipulate objects with complex geometries and contact dynamics. Using a set of four nested buckets from the Yale-CMU-Berkeley Object and Model Set [38], the slave arms must sequentially extract each bucket and place it stably on a surface, avoiding collisions or accidental drops.
- **SIM Card Needle Insertion:** This task replicates a common yet delicate manipulation requiring precise alignment. The slave robot must accurately insert a SIM card needle into the small ejector hole of a mobile phone, then apply the necessary force to release the SIM card tray. This highlights the system’s capacity for fine control in

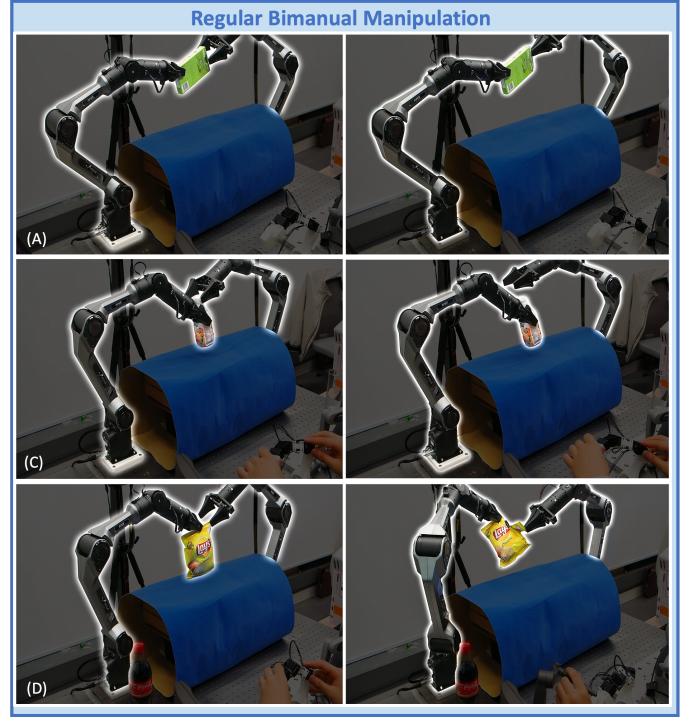


Fig. 8. Snapshots of daily object bimanual manipulation. (A) Opening a snack box. (B) Opening bottle cap. (C) Opening chip bag.

constrained environments.

- **Wire Testing with Multimeter:** This task assesses the system’s ability to perform precise movements in a functional context. The slave robot uses a multimeter to test the conductivity of a Dupont wire by contacting the probes to the small metallic openings on the wire’s connectors. This task underscores the system’s suitability for tasks requiring both precision and tool manipulation.

### C. Large Linear Range Manipulation Demo

To assess the ability of the G-L interface to effectively utilize the entire workspace of the slave robot, we conducted two demonstrations involving large-scale movements spanning the workspace’s full range along the left-right, front-back, and vertical axes. These demonstrations aimed to confirm that the integration of precise manipulation capabilities within the G-L interface did not compromise its capacity for executing large-range manipulation tasks.

- **Object Handling:** This demonstration involved a coordinated bimanual task in which one slave robot retrieved an orange from the far left-front corner of its workspace and transferred it to the second slave robot. The second robot then handed off the orange to a human operator located at the far right-back corner of the workspace. This task exemplifies the system’s ability to facilitate long-range object transfer and cooperative manipulation, similar to demonstrations in prior teleoperation systems [29].
- **Pick and Place from a Cabinet:** This demonstration involved interacting with a tall cabinet positioned behind the slave robot. The task required retrieving specific

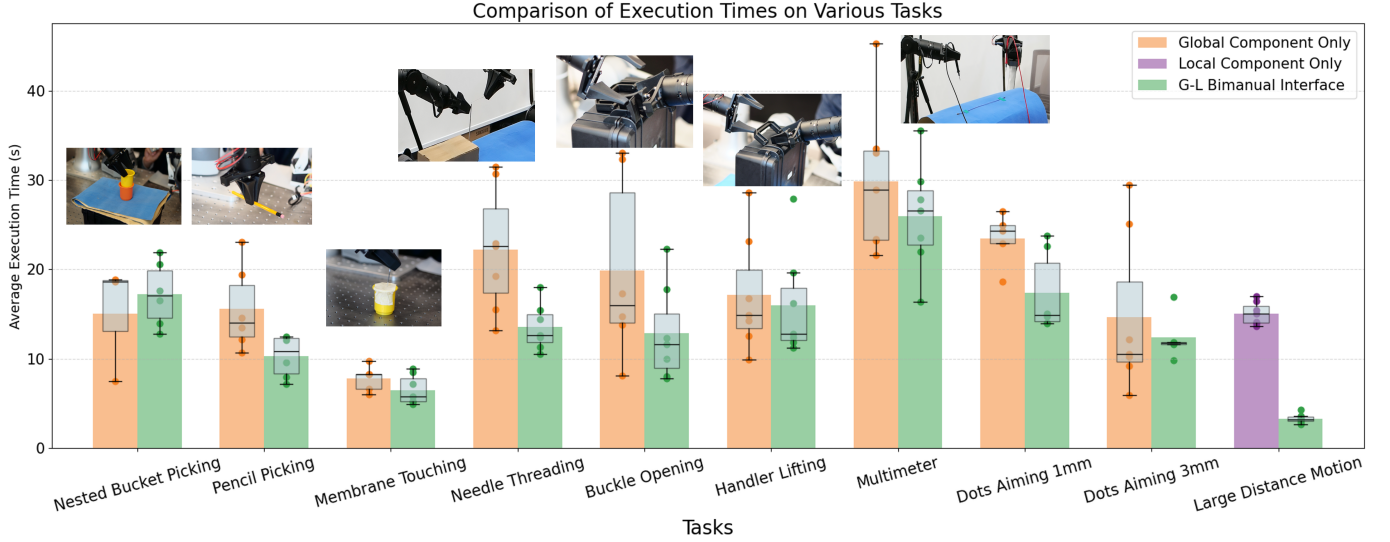


Fig. 9. Comparison of completion time between global component only, local component only, and our proposed G-L interface. The G-L interface outperforms only global component in most tasks, except in the Nested Bucket Picking. As shown in Table I, despite taking less time to complete successful trials, only global component has a significantly lower success rate in Nested Bucket Picking. In large distance motion, G-L interface significantly outperforms local component only.

TABLE I  
SUCCESS RATES OF ISOLATED GLOBAL COMPONENT AND G-L INTERFACE  
ACROSS DIFFERENT TASKS. TASKS ARE SELECTED BASED ON PREDEFINED  
FAILURE CRITERIA DESCRIBED IN SECTION VI-B.

Task	Global Component	G-L Interface
Nested Bucket Picking	3/7	6/7
Pencil Picking	7/7	7/7
Membrane Touching	5/7	7/7
Buckle Opening	6/7	7/7
Handle Lifting	7/7	7/7

objects from a cluttered arrangement within the cabinet and placing them in front of the robot, or conversely, placing objects from the workspace into the cabinet. This task highlights the system’s capacity for navigating and manipulating objects within complex, spatially extended environments.

Both tasks are completed successfully and their snapshots are shown in Fig. 7. These tasks are good examples of how global and local components can cooperate to improve user experiences. The global component ensures a large range of motion while the local component enables the operator to make fine adjustments in clustered environments.

#### D. Large Rotational Range Manipulation Demo

To assess the ability of the singularity avoidance mapping on intuitive orientation control and robustness against wrist singularities, we conducted demonstrations involving considerable end-effector orientation change and needs to cross the wrist singularities.

- **Test Tube Pick and Place:** This demonstration involves picking up a flat-laying test tube from a basin, handle it over to another robot arm and place it on a rack. This

task requires significant pitch angle change and passes through 156 and 456 singularities.

- **Liquid Pouring:** This demonstration involves picking up a test tube from the rack, pour the liquid into a beaker and place the test tube rack. This task requires significant yaw angle change.

Both tasks are completed efficiently and their snapshots are shown in Fig. 7D and 7E. These tasks are good examples of how singularity avoidance motion mapping yields intuitive orientation control and robustness against wrist singularities.

#### E. Daily Object Manipulation

We additionally show the G-L interface can also complement bimanual teleoperation tasks involving daily objects as in Fig. 8. These tasks include picking up a plate, where one slave robot must push down one edge to lift up the other, thereby allow another slave robot to pick up the entire plate. Tasks like opening a chip bag, snack box, and water bottle are also included.

#### F. Fine-Grained Task Completion Time Comparisons

To quantitatively assess the performance improvements enabled by the G-L hierarchical teleoperation system, we conducted a comparative study involving three control conditions: (1) using the global component only, (2) using the local component only, and (3) using both the global and local components. Seven participants were recruited to perform a series of representative tasks, each completed twice under every condition. Regrasping and retrying were allowed unless the task was classified as a failure based on predefined criteria (detailed below). Failed trials were excluded from the computation of average completion time.

Prior to the experiment, all participants received a brief tutorial on system operation and were allotted one hour of

practice to familiarize themselves with the interface and task procedures. For each trial, the master and slave systems were reset to identical initial configurations, and the task completion time was recorded.

Snapshots of the following tasks designed for assessment can be found in the supplementary materials. In addition, the **Needle Threading** and **Wire Testing with Multimeter** are also included. As both tasks have no failure criteria, participants made continuous attempts until successful.

- **Nested Bucket Picking:** Two nested bins were placed on a desk. Participants were tasked with lifting the inner bin without disturbing the outer bin. If either bin fell off the desk during the manipulation, the task was considered to be failed.
- **Pencil Picking:** Participants were tasked with picking up a pencil from a random location on a desk using the slave robot. Contacting the desk with excessive force using the robot gripper resulted in task failure. The pencil's position was randomized for each trial, but participants were allowed to practice with a pencil beforehand.
- **Membrane Touching:** A thin piece of scotch tape, simulating a delicate membrane, was placed over the opening of a small cup. Participants were instructed to bring the needle held by the slave robot into contact with the membrane without puncturing it. Penetration constituted task failure.
- **Buckle Opening:** Participants were asked to open a buckle on a box to open it using the slave robot. Since this task involves close and tight contact with an object, emergency stop of the Piper robot can be triggered if the joint torque exceeds its safety limit. The task was considered failed if the emergency stop is triggered.
- **Handle Lifting:** Participants rotate a laid-down box handle to an upright position and lift the box. Failure conditions are identical to the Buckle Opening task.
- **Dots Aiming:** Abstracting common insertion tasks (e.g., SIM ejector, shafts), participants use the slave gripper to prick three target dots (1 mm and 3 mm radius) with a needle. The target sheet's location is hidden during trials but available for practice. No failure criterion; continuous attempts are allowed until success.
- **Large Distance Motion:** This task compares the G–L interface with a local-only teleoperation setup to evaluate efficiency in executing large-range movements. When repeatedly performing such motions, the G–L interface demonstrates a clear advantage in operational efficiency. Specifically, the G–L interface achieves a significantly shorter task completion time, averaging only  $3.30 \pm 0.53$  seconds, compared to  $15.1 \pm 1.3$  seconds using the local component alone.

Fig. 9 presents the results of the quantitative study, demonstrating that the G–L interface consistently outperforms the isolated global or local components across most tasks. While participants using all configurations were able to quickly move the slave robot's end-effector near the target area, those operating with the global-only setup frequently struggled to perform the final fine motions required for task completion. In

contrast, the local component within the G–L interface enabled smoother and more efficient fine-tuning, resulting in significantly shorter overall completion times. The isolated global component system demonstrated marginally faster completion in nested bucket picking. However, it has a considerably lower success rate comparing to the G–L interface, as elaborated in Table I.

## VII. CONCLUSION, LIMITATIONS, AND FUTURE WORK

This paper presents the Global–Local (G–L) teleoperation interface, which decouples large-scale positioning and fine manipulation through a hierarchical dual-mode control framework. We implemented both direct and singularity-avoiding motion mapping strategies, and introduced the concept of an operational Jacobian to analyze the smoothness and stability of joint behavior during local control. Experimental results across a range of tasks—including precision placement, large workspace traversal, and bimanual manipulation—demonstrate that the G–L interface improves efficiency, task success rate, and user experience compared to conventional global-only or local-only systems.

Nonetheless, several limitations remain. Manual mode switching introduces operational friction and may increase cognitive load. The current singularity-avoiding mapping strategy is task-driven and heuristic, lacking general optimality or theoretical uniqueness. Additionally, the system does not yet support force–torque feedback, and has not been validated under remote or delayed network conditions. Furthermore, the G–L interface's modular architecture supports flexible combinations of global and local master devices, making it broadly adaptable to various application scenarios beyond the current implementation.

Future work will focus on integrating automatic or learning-based switching mechanisms, increasing the system's degrees of freedom to improve singularity robustness, and incorporating visual and force–torque feedback for closed-loop, compliant control. We also plan to extend the operational Jacobian framework to accommodate non-Pieper structures and redundant manipulators, enabling broader applicability and more adaptive mapping strategies. These developments aim to further enhance the robustness, responsiveness, and scalability of the G–L teleoperation interface for real-world deployment in industrial, surgical, and exploratory environments.

## REFERENCES

- [1] J. Vertut, *Teleoperation and robotics: applications and technology*. Springer Science & Business Media, 2013, vol. 3.
- [2] T. Haidegger, J. Sándor, and Z. Benyó, "Surgery in space: The future of robotic telesurgery," *Surgical Endoscopy*, vol. 25, pp. 681–690, 2011.
- [3] G. Brantner and O. Khatib, "Controlling ocean one: Human-robot collaboration for deep-sea manipulation," *Journal of Field Robotics*, vol. 38, no. 1, pp. 28–51, 2021.
- [4] T. B. Sheridan, "Space teleoperation through time delay: Review and prognosis," *IEEE Transactions on Robotics and Automation*, vol. 9, no. 5, pp. 592–606, 1993.
- [5] W.-K. Yoon, T. Goshozono, H. Kawabe, M. Kinami, Y. Tsumaki, M. Uchiyama, M. Oda, and T. Doi, "Model-based space robot teleoperation of ets-vii manipulator," *IEEE Transactions on Robotics and Automation*, vol. 20, no. 3, pp. 602–612, 2004.

- [6] K. D. Katyal, C. Y. Brown, S. A. Hechtman, M. P. Para, T. G. McGee, K. C. Wolfe, R. J. Murphy, M. D. Kutzer, E. W. Tunstel, M. P. McLoughlin *et al.*, "Approaches to robotic teleoperation in a disaster scenario: From supervised autonomy to direct control," in *IEEE/RSJ International Conference on Intelligent Robots and Systems*, 2014.
- [7] I. S. Cardenas and J.-H. Kim, "Design of a semi-humanoid telepresence robot for plant disaster response and prevention," in *IEEE/RSJ International Conference on Intelligent Robots and Systems*, 2019.
- [8] J. Ramos and S. Kim, "Dynamic locomotion synchronization of bipedal robot and human operator via bilateral feedback teleoperation," *Science Robotics*, vol. 4, no. 35, p. eaav4282, 2019.
- [9] Z. Fu, T. Z. Zhao, and C. Finn, "Mobile aloha: Learning bimanual mobile manipulation with low-cost whole-body teleoperation," in *Conference on Robot Learning*, 2024.
- [10] B. Zitkovich, T. Yu, S. Xu, P. Xu, T. Xiao, F. Xia, J. Wu, P. Wohlhart, S. Welker, A. Wahid *et al.*, "Rt-2: Vision-language-action models transfer web knowledge to robotic control," in *Conference on Robot Learning*, 2023.
- [11] K. Darvish, L. Penco, J. Ramos, R. Cisneros, J. Pratt, E. Yoshida, S. Ivaldi, and D. Pucci, "Teleoperation of humanoid robots: A survey," *IEEE Transactions on Robotics*, vol. 39, no. 3, pp. 1706–1727, 2023.
- [12] C. Chi, Z. Xu, S. Feng, E. Cousineau, Y. Du, B. Burchfiel, R. Tedrake, and S. Song, "Diffusion policy: Visuomotor policy learning via action diffusion," *The International Journal of Robotics Research*, p. 02783649241273668, 2023.
- [13] J. Huang, K. Chen, J. Zhou, X. Lin, P. Abbeel, Q. Dou, and Y. Liu, "Dih-tele: Dexterous in-hand teleoperation framework for learning multi-objects manipulation with tactile sensing," *IEEE Transactions on Mechatronics*, 2025.
- [14] B. D. Argall, S. Chernova, M. Veloso, and B. Browning, "A survey of robot learning from demonstration," *Robotics and autonomous systems*, vol. 57, no. 5, pp. 469–483, 2009.
- [15] T. Zhang, Z. McCarthy, O. Jow, D. Lee, X. Chen, K. Goldberg, and P. Abbeel, "Deep imitation learning for complex manipulation tasks from virtual reality teleoperation," in *IEEE International Conference on Robotics and Automation*, 2018.
- [16] Q. Vuong, S. Levine, H. R. Walke, K. Pertsch, A. Singh, R. Doshi, C. Xu, J. Luo, L. Tan, and D. e. a. Shah, "Open x-embodiment: Robotic learning datasets and rt-x models," in *Conference on Robot Learning*, 2023.
- [17] M. Selvaggio, J. Cacace, C. Pacchierotti, F. Ruggiero, and P. R. Giordano, "A shared-control teleoperation architecture for nonprehensile object transportation," *IEEE Transactions on Robotics*, vol. 38, no. 1, pp. 569–583, 2021.
- [18] S. Dass, W. Ai, Y. Jiang, S. Singh, J. Hu, R. Zhang, P. Stone, B. Abbatematteo, and R. Martin-Martin, "Telemona: A modular and versatile teleoperation system for mobile manipulation," in *IEEE International Conference on Robotics and Automation, Workshop on Mobile Manipulation and Embodied Intelligence*, 2024.
- [19] A. Iyer, Z. Peng, Y. Dai, I. Guzey, S. Haldar, S. Chintala, and L. Pinto, "Open teach: A versatile teleoperation system for robotic manipulation," in *Conference on Robot Learning*, 2024.
- [20] X. Cheng, J. Li, S. Yang, G. Yang, and X. Wang, "Open-television: Teleoperation with immersive active visual feedback," in *Conference on Robot Learning*, 2024.
- [21] R. Ding, Y. Qin, J. Zhu, C. Jia, S. Yang, R. Yang, X. Qi, and X. Wang, "Bunny-visionpro: Real-time bimanual dexterous teleoperation for imitation learning," *arXiv preprint arXiv:2407.03162*, 2024.
- [22] Y. Park, J. S. Bhatia, L. Ankile, and P. Agrawal, "Dexhub and dart: Towards internet scale robot data collection," in *Conference on Robot Learning, Workshop on Whole-body Control and Bimanual Manipulation: Applications in Humanoids and Beyond*, 2024.
- [23] Y. Qin, W. Yang, B. Huang, K. Van Wyk, H. Su, X. Wang, Y.-W. Chao, and D. Fox, "Anyteleop: A general vision-based dexterous robot arm-hand teleoperation system," in *Robotics: Science and Systems*, 2023.
- [24] T. Lin, Y. Zhang, Q. Li, H. Qi, B. Yi, S. Levine, and J. Malik, "Learning visuotactile skills with two multifingered hands," in *IEEE International Conference on Robotics and Automation*, 2025.
- [25] S. Yang, M. Liu, Y. Qin, R. Ding, J. Li, X. Cheng, R. Yang, S. Yi, and X. Wang, "Ace: A cross-platform visual-exoskeletons system for low-cost dexterous teleoperation," in *Conference on Robot Learning*, 2024.
- [26] Trossen Robotics, "Mobile AI Robot Arm," <https://www.trossenrobotics.com/mobile-ai>, 2025, accessed: May 1, 2025.
- [27] V. Kumar, Y. V. Hote, and S. Jain, "Review of exoskeleton: History, design and control," in *IEEE International Conference on Recent Developments in Control, Automation and Power Engineering*, 2019.
- [28] P. Tran, S. Jeong, K. R. Herrin, and J. P. Desai, "Hand exoskeleton systems, clinical rehabilitation practices, and future prospects," *IEEE Transactions on Medical Robotics and Bionics*, vol. 3, no. 3, pp. 606–622, 2021.
- [29] P. Wu, Y. Shentu, Z. Yi, X. Lin, and P. Abbeel, "Gello: A general, low-cost, and intuitive teleoperation framework for robot manipulators," in *IEEE/RSJ International Conference on Intelligent Robots and Systems*, 2024.
- [30] J. Aldaco, T. Armstrong, R. Baruch, J. Bingham, S. Chan, K. Draper, D. Dwibedi, C. Finn, P. Florence, S. Goodrich *et al.*, "Aloha 2: An enhanced low-cost hardware for bimanual teleoperation," *arXiv preprint arXiv:2405.02292*, 2024.
- [31] H. Fang, H.-S. Fang, Y. Wang, J. Ren, J. Chen, R. Zhang, W. Wang, and C. Lu, "Airexo: Low-cost exoskeletons for learning whole-arm manipulation in the wild," in *IEEE International Conference on Robotics and Automation*, 2024.
- [32] D. L. Pieper, *The kinematics of manipulators under computer control*. Stanford University, 1969.
- [33] J. Zhou, X. Chen, U. Chang, Y. Liu, Y. Chen, and Z. Wang, "A grasping component mapping approach for soft robotic end-effector control," in *2019 2nd IEEE International Conference on Soft Robotics (RoboSoft)*. IEEE, April 2019, pp. 650–655.
- [34] W. Chen, J. Zhou, S. S. Cheng, Y. Lu, F. Zhong, Y. Gao, and Y. Liu, "Tele-operated oropharyngeal swab (toos) robot enabled by tss soft hand for safe and effective sampling," *IEEE Transactions on Medical Robotics and Bionics*, vol. 3, no. 4, pp. 1040–1053, 2021.
- [35] J. Zhou, W. Chen, S. S. Cheng, L. Xue, M. C. Tong, and Y. Liu, "Bio-inspired soft (bis) hand for tele-operated covid-19 oropharyngeal (op) swab sampling," in *2021 IEEE International Conference on Robotics and Biomimetics (ROBIO)*. IEEE, December 2021, pp. 80–86.
- [36] S. Bruno, S. Lorenzo, V. Luigi, and O. Giuseppe, "Robotics: modelling, planning and control, ch. 3.3," 2010.
- [37] J. Zhou, H. Cao, W. Chen, S. S. Cheng, and Y. Liu, "Bioinspired soft wrist based on multicable jamming with hybrid motion and stiffness control for dexterous manipulation," *IEEE/ASME Transactions on Mechatronics*, vol. 28, no. 3, pp. 1256–1267, 2022.
- [38] B. Calli, A. Singh, J. Bruce, A. Walsman, K. Konolige, S. Srinivasa, P. Abbeel, and A. M. Dollar, "Yale-cmu-berkeley dataset for robotic manipulation research," *The International Journal of Robotics Research*, vol. 36, no. 3, pp. 261–268, 2017.